# THRUSTER POINTING CONSTRAINED OPTIMAL 6-DOF PROXIMITY OPERATIONS USING INDIRECT OPTIMIZATION

## Himmat Panag\*, Ruthvik Bommena\*, and Robyn Woollands\*

Future space missions, such as in-space telescope assembly and on-orbit servicing, require rendezvous and proximity operations that avoid thruster-induced contamination and plume impingement on sensitive components of the client spacecraft. In this paper, we introduce a novel thruster pointing constraint into the six degreesof-freedom (6DOF) optimal rendezvous problem and solve it using indirect optimization techniques. A thruster pointing constraint limits the angular range over which a spacecraft's thrusters may operate, thereby avoiding plume contamination while still minimizing the desired objection function (e.g. fuel consumption or time-of-flight). By embedding this constraint directly into the dynamical model, our solution method eliminates the need for prior knowledge of the burn sequence or the precise times at which the constraint transitions to active/inactive. The spacecraft's 6-DOF motion is controlled by a set of fixed translational thrusters and an attitude control system that can provide instantaneous torque. Our solution method is demonstrated for an orbit rendezvous problem considering the Clohessy-Wiltshire relative dynamics for the translational motion and modified Rodrigues parameters for the attitude motion. A validation is presented through comparison with solutions to the simpler 3DOF problem.

#### INTRODUCTION

Rendezvous, proximity operations, and docking (RPOD) are essential elements of many upcoming space missions, including cargo delivery, refueling, inspection, and in-space assembly. Advances in reusable rockets, enhanced flight computer processing power, and the push for sustainable space operations have sparked renewed interest in on-orbit servicing and manufacturing (OSAM) missions, also referred to as ISAM. A typical scenario involves a chaser spacecraft performing maneuvers in close proximity to a target spacecraft. In such situations, it is crucial to consider the potential impact of exhaust plumes from thrusters, which can induce contamination and undesired forces and torques on the target spacecraft. This is especially critical when the target spacecraft carries sensitive payloads, such as a space telescope or star tracker, where plume impingement can significantly jeopardize mission success. While using inert gas thrusters can help mitigate contamination by design, they are inefficient and still contribute to plume impingement. An alternative approach explored in this work is the introduction of a thruster pointing constraint, which limits the angular range in which thrusters can operate. This constraint helps reduce both plume impingement and contamination, however, the constraint is nonlinear, discontinuous, and varies with the relative position and orientation of the chaser spacecraft, making the resulting optimal control problem particularly challenging to solve.

<sup>\*</sup>PhD Student, Department of Aerospace Engineering, hpanag2@illinois.edu

<sup>†</sup>PhD Student, Department of Aerospace Engineering, rbomme2@illinois.edu

<sup>&</sup>lt;sup>‡</sup>Assistant Professor, Department of Aerospace Engineering, rmw@illinois.edu

Two approaches are typically used to solve these optimal control problems: Direct and Indirect methods. Direct methods involve discretizing and parameterizing the states and controls using a set of basis functions. This results in a large nonlinear programming problem, which is then solved through an iterative procedure. This method does not guarantee an optimal solution. In contrast, indirect methods focus on finding solutions by solving for the necessary conditions of local optimality, derived from Pontryagin's Maximum Principle. These necessary conditions lead to a two-point boundary value problem, where the unknown initial costates are determined using single or multiple shooting methods to satisfy the final state boundary conditions. While indirect methods are effective at handling nonlinearities and ensure local optimality, they are often highly sensitive to the initial guess and typically require smoothing and continuation techniques to arrive at the final solution.

The thruster-pointing constrained optimal transfer problem has received attention in recent years with a direct sequential convex optimization approach applied to both 3DOF<sup>2</sup> and 6DOF<sup>3</sup> cases. These methods address the nonconvexities in the constraints and dynamics through linearization. The problem is then discretized into a nonlinear programming problem and solved using a method of successive approximations. However, the reliance of these approaches on linearizing the highlynonlinear rotational dynamics severely limits their utility. In the context of indirect methods, the constrained 3DOF problem is typically approached in two ways. One approach, as discussed in,<sup>5</sup> involves augmenting the cost functional with an integral penalty barrier function. While this barrier function method is general and powerful, it can suffer from slow convergence and implementation complexity. The second approach, outlined in. erlies on knowledge of the sequence of constrained and unconstrained arcs. It solves for these arcs and applies the Weierstrass-Erdmann corner conditions at the junction points to piece together the optimal solution. This method is faster to compute but lacks scalability, as the optimal burn sequence is generally not known in advance. More recently, Panag & Woollands, solved the problem by reparameterizing the control set to smoothly embed the constraint into the state dynamics. In this approach, the control set of the resulting optimal control problem is fixed, allowing the problem to be solved as though it were an unconstrained 3DOF problem.

The 6DOF problem is important to proximity operations for several reasons. Firstly, limits on spacecraft angular accelerations are naturally incorporated into the 6DOF problem by limiting the available control torque. Furthermore, during proximity operations position and attitude are often coupled, and both need to be controlled simultaneously throughout the trajectory. The attitude of the spacecraft may be represented by various attitude parameterizations. Most commonly employed are Euler Angles (which suffer from singularities), quaternions and rotation matrices (which are non-minimal and require additional constraints to be satisfied, unit quaternion norm and matrix orthogonality respectively), and Modified Rodrigues Parameters (MRP) which represent each attitude using two sets (standard and shadow), and are the parameterization used in this paper. It is important to note that MRPs are discontinuous when switching between the standard and shadow set, and thus the corresponding MRP costate switching condition (derived in [10]) must be introduced in order to formulate the OCP.

Irrespective of the formulation chosen, the rotational dynamics are highly nonlinear, making direct approaches unsuitable. While indirect methods can handle these nonlinearities, spacecraft reorientation problems in which the control appears linearly in the Hamiltonian often suffer from singular arcs for the control torque, <sup>11,12</sup> which occur when the necessary conditions obtained from PMP do not provide enough information to determine the optimal control. While control torque is

often penalized in 6DOF transfer problems, <sup>13</sup> in this work we assume that objective is to minimize fuel consumption only, giving rise to singular controls.

Singular controls can be treated by various regularization techniques which modify the dynamics,  $^{14,15}$  cost function  $^{16}$  or both by a small factor (say  $\gamma$ ). While it is not always practical to trace these homotopies, it can be shown that solutions to the modified OCP converge to solutions of the original OCP as  $\gamma \to 0$ . The Epsilon-Trig regularization method relies on appending one control term to the state dynamics and replacing the bounded control  $-1 \le u \le 1$  with a trigonometric function  $\sin u_{TRIG}$ , however it encounters numerical issues if both switch function and costate are simultaneously near zero. The  $\epsilon$  – algorithm, adds a quadratic control term to the running cost in order to remove the singular arc. While this approach yields good initial convergence, our experiments showed that it was difficult to reduce the factor sufficiently to approximate the singular arc. These methods require altering the system dynamics, which in turn modifies the Hamiltonian and costate equations, making them expensive and complex to implement. More recently, the Unified Trigonometric Method (UTM) uses trigonomometrization of the control and appends an orthogonal control term to the running cost only. This requires no modification to the implementation, except for inclusion of an L2 norm-based regularization smoothing function.

The main contribution of this paper is the development of an indirect optimization framework to solve the 6DOF thruster-pointing-constrained problem. Plume models suggest that approximately 99% of the engine exhaust mass is concentrated within  $10^\circ$  of the plume centerline. While the specific choice of constraint region is left to the mission designer, it's important to note that overly restrictive constraints can make the desired final state unreachable. In this work, we do not address the question of reachability and instead assume that the constrained problem is feasible. Our approach incorporates continuation and smoothing techniques to gradually enforce the pointing constraints within the iterative solution process. To address the challenge of singular arcs, we implement the L2 norm-based regularization approach within the optimization scheme. We demonstrate the effectiveness of our method on a 6DOF spacecraft rendezvous scenario and validate the results using a convex optimization solver.

The paper is organized as follows: We first introduce the dynamical models used to formulate the problem, including the incorporation of the shadow sew for the MRPs. We then formulate the unconstrained optimal control problem, introduce the homotopy and continuation techniques used and describe how singular arcs are treated. Following this we modify the dynamics to include the thruster pointing constraint and present various results, including a comparison to the simpler constrained 3DOF problem.

### DYNAMICAL MODEL

The constrained thruster pointing approach developed in this paper can be applied to any set of dynamical equations whose origin is collocated with the target spacecraft. Let the relative dynamics of the region be given by f(x). To model spacecraft maneuvers, a perturbing thrust term for each engine is added to the dynamics as well as an additional equation to keep track of the spacecraft mass as propellant is consumed. A single control torque term,  $\tau$  is added to the rotational dynamics to capture the control authority of a reaction wheel system. The attitude is expressed using Modified Rodrigues Parameters, p, with respect to an inertial frame. The equations of motion for the system

then become:

$$\dot{r} = v \tag{1}$$

$$\dot{m} = -\frac{T}{c} \sum_{i=1}^{n} \delta_i \tag{2}$$

$$\dot{\boldsymbol{v}} = f(\boldsymbol{x}) + \frac{T}{m} \sum_{i=1}^{n} \delta_i \boldsymbol{\Psi}(\boldsymbol{p}, t) \boldsymbol{u_i}$$
(3)

$$\dot{\boldsymbol{p}} = \frac{1}{4} \left[ \left( 1 + |\boldsymbol{p}|^2 \right) I_{3\times 3} + 2 \left[ \boldsymbol{p} \times \right]^2 + 2 \left[ \boldsymbol{p} \times \right] \right] \boldsymbol{\omega}, \text{ where } \left[ \boldsymbol{p} \times \right] = \begin{bmatrix} 0 & -p_3 & p_2 \\ p_3 & 0 & -p_1 \\ -p_2 & p_1 & 0 \end{bmatrix}$$
(4)

$$I\dot{\omega} = -\omega \times (I\omega) + T\sum_{i=1}^{n} \delta_i (d_i \times u_i) + \tau,$$
 (5)

where T is the maximum thrust available from each engine, c is the exhaust velocity, m is the mass of the chaser spacecraft, the subscript i denotes the  $i^{th}$  engine,  $\delta_i$  is the engine throttle,  $\Psi(\boldsymbol{p},t)$  is a direction cosine matrix (DCM) which transforms vectors from the chaser body frame into the translational dynamics frame,  $\boldsymbol{u_i}$  is a unit vector in the direction of thrust (opposite to the plume), expressed in the body frame of the chaser and  $\boldsymbol{d_i}$  is the location of engine i expressed in the body frame. In this work we assume that the chaser is a cube of side length 1m.

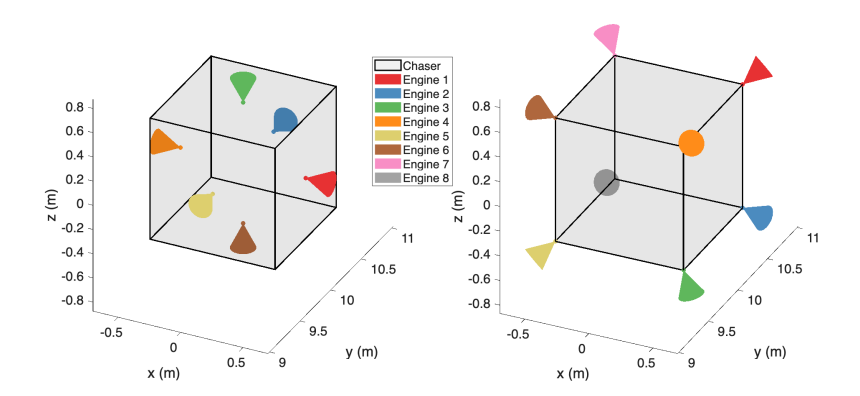


**Figure 1**: Chaser spacecraft with two example thruster configurations. The thrust vectors are aligned with the center of mass (COM) of the chaser.

For the translational dynamics, we utilize the Clohessy-Wiltshire  $(CW)^{19}$  equations, a set of linearized equations describing the relative motion between two objects in close proximity under the influence of a central gravitational force when the target vehicle is assumed to be in a circular orbit. The frame for the CW equations is the LVLH (local-vertical-local-horizontal) frame, where the x axis is pointing radially outward from the Earth to the target spacecraft, the y axis is in the velocity direction and z axis is oriented in the direction of the angular momentum vector. In order to maintain this definition, the frame rotates at a constant rate,  $\Omega$  about its z axis. Therefore the rotation matrix  $\Psi(p,t)$  can be written as follows:

$$\Psi(\mathbf{p}, t) = \text{DCM}_{\text{Inertial} \to \text{LVLH}}(t) \text{DCM}_{\text{Body} \to \text{Inertial}}(\mathbf{p}). \tag{6}$$

The rotation matrix from the body frame to the inertial frame is given by, <sup>20</sup>

$$DCM_{Body \rightarrow Inertial}(\boldsymbol{p}) = I - \frac{4(1 - |\boldsymbol{p}|^2)}{(1 + |\boldsymbol{p}|^2)^2} [\boldsymbol{p} \times] + \frac{8}{(1 + |\boldsymbol{p}|^2)^2} [\boldsymbol{p} \times]^2.$$
 (7)

Finally, due to the constant rotation rate of the LVLH frame, the rotation matrix from the Inertial to LVLH frame is given by:

$$DCM_{Inertial \to LVLH}(t) = \begin{bmatrix} \cos(\Omega t) & \sin(\Omega t) & 0\\ -\sin(\Omega t) & \cos(\Omega t) & 0\\ 0 & 0 & 1 \end{bmatrix}.$$
 (8)

Propagation of the dynamics is done using a numerical integrator. Further details about the CW equations can be found in most orbital mechanics textbooks (e.g. Curtis<sup>21</sup>).

#### **Shadow Set for MRPs**

To avoid the singularity of the original MRP at principal rotation angles of  $360^{\circ}$ , a switching surface defined by  $p^{T}p = k$  is implemented in MATLAB using event detection (k is set to a value slightly above 1 to avoid chattering). When the switching surface is hit, the integration is stopped and the MRP is replaced with its equivalent from the shadow set. This discontinuity also requires replacing the MRP costate.  $^{10}$ 

$$p^S = -\frac{p}{p^T p} \tag{9}$$

$$\boldsymbol{\lambda}_{\boldsymbol{p}}^{S} = \left[2\boldsymbol{p}\boldsymbol{p}^{\mathrm{T}} - (\boldsymbol{p}^{\mathrm{T}}\boldsymbol{p})I\right]\boldsymbol{\lambda}_{\boldsymbol{p}},\tag{10}$$

where the superscript  $^S$  denotes the value of the state/costate after the switch function. The other states and costates remain unchanged and the integration is continued until the final time is reached.

## FORMULATION OF THE FUEL-OPTIMAL CONTROL PROBLEM

In this section we first formulate the unconstrained fuel-optimal control problem by applying primer vector theory.<sup>22</sup> We then incorporate the thruster pointing constraint using a homotopy, which reduces a thruster's effectiveness if it is directed at the target by a factor  $\eta$ .

#### **Unconstrained Fuel-Optimal Formulation**

The cost functional (J) for minimizing the total propellant mass consumed in a fixed time-of-flight can be written as

$$J(\boldsymbol{\delta}) = \frac{T}{c} \int_0^{t_f} \sum_{i=1}^n \delta_i dt.$$
 (11)

For a solution to be at least locally optimal, Pontryagin's Maximum Principle<sup>1</sup> must be satisfied. That is, the Hamiltonian must be minimized pointwise in time over the set of all permissible controls to drive a dynamical system from the initial to the final state. The Hamiltonian can be written as

$$H = \frac{T}{c} \sum_{i=1}^{n} \delta_{i} \left[ 1 + \frac{c}{m} \boldsymbol{\lambda}_{\boldsymbol{v}}^{\mathrm{T}} \boldsymbol{\Psi}(\boldsymbol{p}, t) \boldsymbol{u}_{i} - \lambda_{m} + c \boldsymbol{\lambda}_{\boldsymbol{\omega}}^{\mathrm{T}} \boldsymbol{I}^{-1} \left( \boldsymbol{d}_{i} \times \boldsymbol{u}_{i} \right) \right] + \boldsymbol{\lambda}_{\boldsymbol{\omega}}^{\mathrm{T}} \boldsymbol{I}^{-1} \boldsymbol{\tau} + \dots$$
$$+ \boldsymbol{\lambda}_{\boldsymbol{r}}^{\mathrm{T}} \boldsymbol{v} + \boldsymbol{\lambda}_{\boldsymbol{v}}^{\mathrm{T}} f(\boldsymbol{x}) + \boldsymbol{\lambda}_{\boldsymbol{p}}^{\mathrm{T}} \dot{\boldsymbol{p}} + \boldsymbol{\lambda}_{\boldsymbol{\omega}}^{\mathrm{T}} \boldsymbol{I}^{-1} \left( \boldsymbol{\omega} \times (\boldsymbol{I} \boldsymbol{\omega}) \right)$$
(12)

where  $\lambda_x = [\lambda_r, \lambda_v, \lambda_m, \lambda_p, \lambda_{\omega}]^T$  is the vector of costates. The necessary conditions for optimality (costate dynamics) are obtained using the Euler-Lagrange relation as follows:

$$\dot{\lambda}_{x} = -\frac{\partial H}{\partial \mathbf{r}},\tag{13}$$

where  $x[r, v, \lambda_m, p, \omega]^T$ . Note that all of the controls terms are contained in Eq. 12. The optimal choice (superscript "\*") of the throttle of engine i is given by:

$$\delta_i^* = \arg\min_{0 \le \delta_i \le 1} H = \frac{1}{2} \left( 1 + \operatorname{sign}(S_i) \right), \tag{14}$$

where 
$$S_i = \lambda_m - 1 - \frac{c}{m} \boldsymbol{\lambda}_v^{\mathrm{T}} \boldsymbol{\Psi}(\boldsymbol{p}, t) \boldsymbol{u}_i - c \boldsymbol{\lambda}_\omega^{\mathrm{T}} \boldsymbol{I}^{-1} (\boldsymbol{d}_i \times \boldsymbol{u}_i)$$
 (15)

Similarly each component of the control torque au is chosen independently to minimize the Hamiltonian

$$\tau_{j}^{*} = \underset{|\tau_{j}| < \tau_{\text{max}}}{\min} H = -\tau_{\text{max}} \operatorname{sign} \left( \boldsymbol{\lambda}_{\boldsymbol{\omega}}^{\mathrm{T}} \boldsymbol{I}^{-1} \right)_{j} \quad j = 1, 2, 3.$$
(16)

Note that the Maximum Principle only requires  $\tau$  to be piecewise continuous, so there is no restriction on how fast  $\tau$  can change. This assumption may not be realistic for some attitude control systems, at which point it would be necessary to include the reaction wheel dynamics into the problem formulation. In this analysis, we assume that the control system is not near saturation and can provide instantaneous (finite) torques in all directions. For a fixed-time rendezvous problem, the final conditions can be written in the form of thirteen equality constraints,

$$\begin{bmatrix} \boldsymbol{x}(t_f) - \boldsymbol{x}_F \\ \lambda_m(t_f) \end{bmatrix} = \boldsymbol{0}. \tag{17}$$

Note, the above equation should be scaled so that the magnitude of each equation is approximately representative of the desirable relative errors in any solution. For example, a  $1^{\circ}$  error in attitude may be deemed of the same significance as a 1mm error in position. By scaling the MRP and position error equation accordingly, we can further aid the solver in deciding which direction to optimize in. The state/costate dynamics for the fuel-optimal, fixed-time, optimal control problem can be written as follows.

$$\dot{X} = \begin{bmatrix} \dot{x} \\ \dot{\lambda} \end{bmatrix}, \tag{18}$$

where  $\tau = \tau^*$  and  $\delta_i = \delta_i^*(S_i, \rho)$  are used in the RHS of Eq. (18). Numerical integration of the equations of motion with the known initial states  $x(t_0) = x_0$  and unknown initial costates  $\lambda(t_0)$  are required to solve the two point boundary value problem such that Eq. (17) is satisfied.

## **Homotopy and Continuation Techniques**

We use a hyperbolic tangent smoothing function to approximate the engine throttle step input as shown below. The continuation parameter,  $\rho$ , is swept from 1 to  $1\times 10^{-5}$ , and clearly, as  $\rho\to 0$  the hyperbolic tangent function approximates the sign() function. Using a hyperbolic tangent smoothing function aids the numerical convergence for this bang-bang type optimal control problem. More details on the hyperbolic tangent smoothing function are presented in [23] and [24].

$$\delta_i^*(S_i) = \frac{1}{2} \left[ 1 + \operatorname{sign}(S_i) \right] \cong \delta_i^*(S, \rho) = \frac{1}{2} \left[ 1 + \tanh\left(\frac{S_i}{\rho}\right) \right] \tag{19}$$

The 6DOF problem is extremely sensitive when the inertia of the spacecraft is small. For example, for a problem consisting of 60° rotation only, any initial guess of the costate easily converges when  $\rho$  is large. We expect the solution to consist of a simple rotation, however upon sweeping  $\rho \to$  $1 \times 10^{-5}$  we find that the spacecraft completed multiple revolutions before settling to the target attitude. While these are valid locally optimal solutions, they are undesirable trajectories. This sensitivity can be overcome with various continuation techniques, such as gradually; reducing the inertia, increasing the allowable control torque, or penalizing control torque.

### **Singular Control Torques**

The minimum-time spacecraft reorientation problem can contain both bang-bang and singular controls due to the control appearing linearly in the Hamiltonian.<sup>25</sup> This occurs when the torque switch function (Eq. 20) is zero on some time intervals of the transfer. This proved to be the case in this problem, and while penalizing the control torque as in the  $\epsilon$ -algorithm<sup>16</sup> provides an approximate way to handle any singular arcs, it is sub-optimal and increasingly difficult to converge trajectories as the penalty term approaches zero. In order to circumvent this, we use L2-norm based regularization<sup>18</sup> to handle bang-bang and singular arcs, as follows:

$$S_{\tau_j} = -\left(\boldsymbol{\lambda}_{\boldsymbol{\omega}}^{\mathrm{T}} \boldsymbol{I}^{-1}\right)_j = \frac{\partial H}{\partial \tau_j}$$
 (20)

$$\tau_j^* = \frac{S_{\tau_j}^2}{\sqrt{S_{\tau_j}^2 + \kappa^2}}. (21)$$

As  $\kappa \to 0$ , Eq. 21 approximates Eq. 16 for large  $|S_{\tau_j}| >> \kappa$  and converges to the singular control otherwise. For a finite order singular arc, the optimal control,  $au_{ ext{singular}}^*$  can be derived by taking the time derivative of the switch function until the control term appears. In this work, we do not analyse the singular arc analytically.

### **Thruster Pointing Constrained Fuel-Optimal Formulation**

We now wish to restrict the control set of the chaser so that its engine plumes do not strike a spherical zone around the target during the transfer as shown in Figure 2. Theoretically, PMP could be applied to choose the optimal (Hamiltonian minimizing) control point-wise in time, from a non-smooth state dependent control set. However, this approach is impractical as fsolve and ode45 require a smooth formulation of the necessary conditions in order to achieve convergence. There are numerous ways to implement a constraint function that is continuous and smooth. One such example is presented in our previous work,<sup>7</sup> however is limited to spherical constraints. In this work we derive a simpler constraint function which can be easily extended to convex solids. Suppose the target has radius R, the equations for a sphere and the ray aligned with the center-line of the  $i^{\text{th}}$  engine plume (in the LVLH frame) are given by equations 22 and 23 respectively. Here,  $\theta$ is a parameter which describes the ray.

$$|r_{sphere}|^2 = R^2 \tag{22}$$

$$r_{ray} = r_i^{\text{LVLH}} + \Psi d_i - \theta \Psi u_i, \theta \ge 0$$
 (23)

$$r_{ray} = r_i^{\text{LVLH}} + \Psi d_i - \theta \Psi u_i, \theta \ge 0$$

$$r_i^{\text{LVLH}}(r, p, t) = \Psi(p, t) d_i + r$$
(23)

$$r_i^{\text{Body}}(r, p, t) = \Psi(p, t)^{\text{T}} r + d_i.$$
 (25)

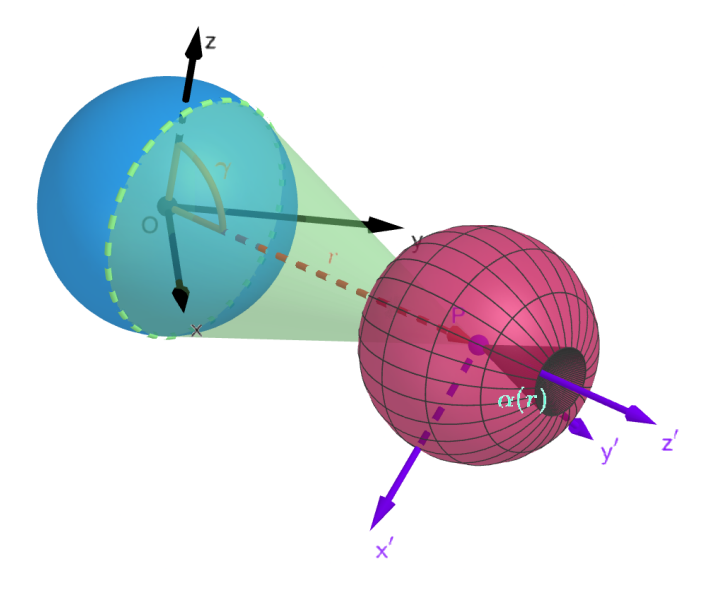


Figure 2: The thruster pointing constraint varies as a function of distance from the spherical target (blue sphere). The red sphere is centered at the  $i^{th}$  engine, if  $u_i$  lies in the green zone, the constraint is activated.

The points of intersection of these two functions are found by solving equations 22 and 23 for  $\theta$ . The resulting quadratic has 0,1, or 2 real solutions, with the constraint being inactive if no real solutions exists. The discriminant of the resulting quadratic equation gives rise to the following constraint function  $E_i$ :

$$E_{i}(\boldsymbol{r},\boldsymbol{p},t) = \begin{cases} \frac{1}{R^{2}} \left( |\boldsymbol{r}|^{2} + 2\boldsymbol{r}^{T}\boldsymbol{\Psi}\boldsymbol{d}_{i} + |\boldsymbol{d}_{i}|^{2} - R^{2} - \left(\boldsymbol{u}_{i}^{T}\boldsymbol{r}_{i}^{\text{Body}}\right)^{2} \right), & \boldsymbol{u}_{i}^{T}\boldsymbol{r}_{i}^{\text{Body}} \geq 0, \\ \frac{1}{R^{2}} \left( |\boldsymbol{r}|^{2} + 2\boldsymbol{r}^{T}\boldsymbol{\Psi}\boldsymbol{d}_{i} + |\boldsymbol{d}_{i}|^{2} - R^{2} \right), & \text{otherwise} \end{cases}$$

$$1 \left[ (E_{i}) \right] \in \mathcal{D} \left\{ 0 \quad \text{constraint violated} \right\}$$
(26)

$$\eta_i(\mathbf{r}, \mathbf{p}, t) = \frac{1}{2} \left[ 1 + \tanh\left(\frac{E_i}{\epsilon}\right) \right] \xrightarrow{\epsilon \to 0} \begin{cases} 0, & \text{constraint violated,} \\ 1, & \text{otherwise.} \end{cases}$$
(27)

Note that Eq. 26 is smooth and differentiable, in which the second case handles negative real solutions of  $\theta$ . Using the constraint function, we define the thruster effectiveness,  $\eta_i$  which smoothly scales the throttle to zero if the constraint is violated. By adding this term into the dynamics, any optimal solution of the problem automatically satisfies the constraint. Like the bang-bang thrust profile, this is a nonlinear phenomenon, which requires a second continuation parameter  $\epsilon$  to aid the solver in convergence. With the definition above, we modify the dynamics equations 2, 3, 5 to

include  $\eta_i$ .

$$\dot{m} = -\frac{T}{c} \sum_{i=1}^{n} \delta_i \eta_i \tag{28}$$

$$\dot{\boldsymbol{v}} = f(\boldsymbol{x}) + \frac{T}{m} \sum_{i=1}^{n} \delta_i \eta_i \boldsymbol{\Psi}(\boldsymbol{p}, t) \boldsymbol{u_i}$$
(29)

$$I\dot{\boldsymbol{\omega}} = -\omega \times (I\omega) + T\sum_{i=1}^{n} \delta_{i}\eta_{i} (\boldsymbol{d_{i}} \times \boldsymbol{u_{i}}) + \boldsymbol{\tau}.$$
 (30)

This causes a change to the Hamiltonian and the equation for the switch function (Eq. 31) becomes:

$$S_{i} = -1 + \eta_{i} \left( \lambda_{m} - \frac{c}{m} \boldsymbol{\lambda}_{v}^{T} \boldsymbol{\Psi}(\boldsymbol{p}, t) \boldsymbol{u}_{i} - c \boldsymbol{\lambda}_{\omega}^{T} \boldsymbol{I}^{-1} \left( \boldsymbol{d}_{i} \times \boldsymbol{u}_{i} \right) \right).$$
(31)

Note, if the cost function is modified to include the  $\eta_i$  term, the switch function would approach zero whenever the constraint was active. This would lead to a singular arc for  $\epsilon \to 0$  and complicates the implementation. Intuitively, if  $\eta_i = 0$ , we expect  $\delta_i^* = 0$  since a non-zero value would have no affect on the dynamics, costate dynamics and serve only to increase the cost. We therefore exclude it from the cost function, and notice that  $S_i = -1$  when  $\eta_i = 0$ .

### **RESULTS**

**Table 1**: Parameters used for simulation

Parameter	Value
Target spacecraft altitude	696km
Mean motion of target, $\Omega$	0.001060923rad/s
Transfer time, $t_f$	48sec
Chaser initial mass, $m(t_0)$	100kg
Maximum Engine Thrust, T	3N
Maximum Control Torque (in each direction), $\tau_i$	0.5Nm
Engine Specific Impulse, $I_{sp}$	300sec
Chaser Inertia, I	diag ( $[36, 37, 38]$ ) kg.m <sup>2</sup>
Initial relative position, $r(t_0)$	$[0, 10, 0]^{\mathrm{T}}$ m
Final relative position, $r(t_f)$	$[0,4,0]^{\mathrm{T}}$ m
Initial and final relative velocity, $\boldsymbol{v}\left(t_{0}\right), \boldsymbol{v}\left(t_{f}\right)$	$[0,0,0]^{\mathrm{T}}$ m/s
Initial and final MRP, $\boldsymbol{p}\left(t_{0}\right)$ , $\boldsymbol{p}\left(t_{f}\right)$	$[0, 0, 0]^{\mathrm{T}}$
Initial and final angular velocity, $\boldsymbol{\omega}\left(t_{0}\right), \boldsymbol{\omega}\left(t_{f}\right)$	$[0,0,0]^{\mathrm{T}}$ rad/s

We consider the problem of rendezvous and proximity operations around a target located in a circular low Earth orbit. The relative motion dynamics are modeled using Clohessy-Wiltshire dynamics in the LVLH frame. In our simulations, the chaser starts 10 metres in front of the target (i.e. in the velocity direction) and it terminates at a position 4 metres in front of the target. Unless specified otherwise, in all simulations a time of flight of 48 seconds is used and the chaser data used to generate the results is given in Table 1. The chaser configuration consists of 6 identical engines, one on each face of a cube of side length 1m. Each engine's thrust direction is aligned with the COM of the spacecraft as shown in Figure 1. Each optimal control problem is solved using single shooting and *MATLAB's ode45* and *fsolve*. The final state error used as the

objective function for *fsolve* was scaled in such a way that errors in position, velocity, orientation and angular velocity of 1mm, 0.1mm/s, 1° and 0.1°/s respectively, had approximately the same magnitude. This helps *fsolve* weight the error contributions more meaningfully and aided in convergence, although is not strictly necessary. The code to generate the results below can be found at https://github.com/himmatpanag/ThrusterPointingConstrainedRPOD.

#### Solutions without control torque

We first present results for the problem without reaction control torque. Since the thrusters are aligned with the COM, the attitude dynamics are not controllable. This is a restrictive assumption, however it illuminates some of the intricacies of the problem and is a good starting point when comparing against previous results.<sup>7</sup> Note, since the attitude dynamics is uncontrollable, the attitude costates  $(\lambda_p, \lambda_\omega)$  are removed from the initial guess to reduce the dimensionality of the search space for *fsolve*. Figure 3 shows the initial and final orientations of the chaser over an unconstrained transfer with engine 5 on and pointing almost directly at the target during the terminal braking burn.

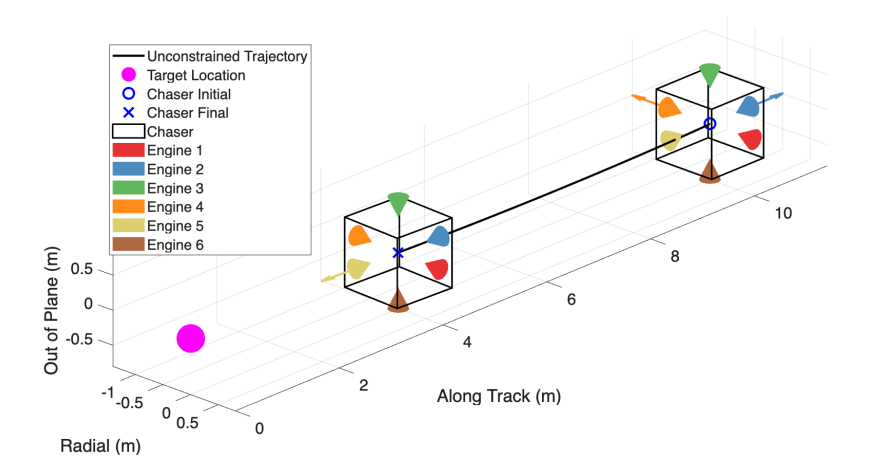


**Figure 3**: Solution of the unconstrained 6DOF problem without control torque showing initial and final orientation

In Figure 4 we see that as the constraint radius is increased the chaser is forced further from the nominal (unconstrained) trajectory to avoid engine 5 firing while pointed at the target during the final burn. Figure 4a shows the plume angle of engine 5 for different target radii. Dashed lines indicate that the engine is off and solid lines indicate that the engine is on. The minimum allowable plume angle corresponding to each target radius is shown in a dash-dot line and it can be seen that, for each transfer, engine 5 is only active at values greater that the minimum allowable plume angle. The corresponding change in shape of the trajectory is shown in Figure 4b. The converged values of the initial costates ( $\lambda_x(0)$ ) for several cases presented in this section are summarized in Table 2. To achieve convergence, we start at  $\epsilon=.2$  and  $\rho=0.4$  before gradually reducing these to small values.

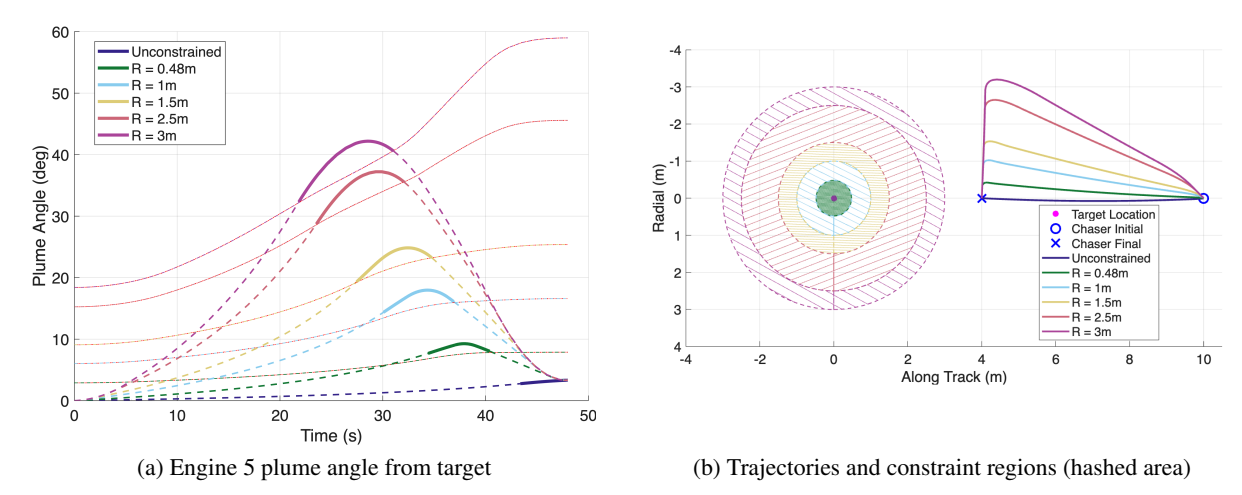


Figure 4: Solutions of the 6DOF problem without control torque with increasing constraint radius.

**Table 2**: Converged initial costates for the single shooting constant constraint angle fuel-optimal problem

Variable	Unconstrained	R = 1.02m	R = 2.5m	R = 3.02m
$\overline{\rho}$	0.00099854	0.00084212	0.01841	0.0097338
$\epsilon$	0.5	0.050353	0.00093571	0.0070538
$\lambda_{r_1}$	-1.36117063	2.35113642	3.4185088	4.26076013
$\lambda_{r_2}$	1.68363843	2.98309447	4.78887926	5.81537138
$\lambda_{r_3}$	-4.89872128e-11	-4.49830699e-07	-6.26982534e-09	4.61516004e-08
$\lambda_{v_1}$	-34.2324575	35.9038924	45.4958453	54.123807
$\lambda_{v_2}$	39.5411119	54.1277672	75.1068362	87.9190385
$\lambda_{v_3}$	-3.97992384e-10	3.19443139e-05	-4.1878299e-08	-1.30022771e-06
$\lambda_m$	0.000101020535	0.00027213008	0.000573912077	0.00076507811
$\lambda_{p_1}$	-8.931051e-06	-8.931051e-06	-8.931051e-06	-8.931051e-06
$\lambda_{p_2}$	-1.093674e-06	-1.093674e-06	-1.093674e-06	-1.093674e-06
$\lambda_{p_r}$	3.52454e-06	3.52454e-06	3.52454e-06	3.52454e-06
$\lambda_{\omega_x}$	-7.1361039e-05	-7.1361039e-05	-7.1361039e-05	-7.1361039e-05
$\lambda_{\omega_y}$	-1.0314917e-05	-1.0314917e-05	-1.0314917e-05	-1.0314917e-05
$\lambda_{\omega_z}$	8.709836e-06	8.709836e-06	8.709836e-06	8.709836e-06

### **Solutions with control torque**

We now solve the problem with a control torque  $\tau \in [-\tau_{max}, \tau_{max}]^3$ , letting each component of torque vary independently. Figure 5 shows the unconstrained trajectory, the thruster-pointing-constrained trajectory without attitude control, and finally, the thruster-pointing-constrained trajectory with attitude control. It is clear that when attitude control is permitted, a much smaller deviation in the trajectory is needed to hit the same final boundary conditions, while also satisfying the specified thruster pointing constraints. The arrows indicate when an engine is on and its plume direction.

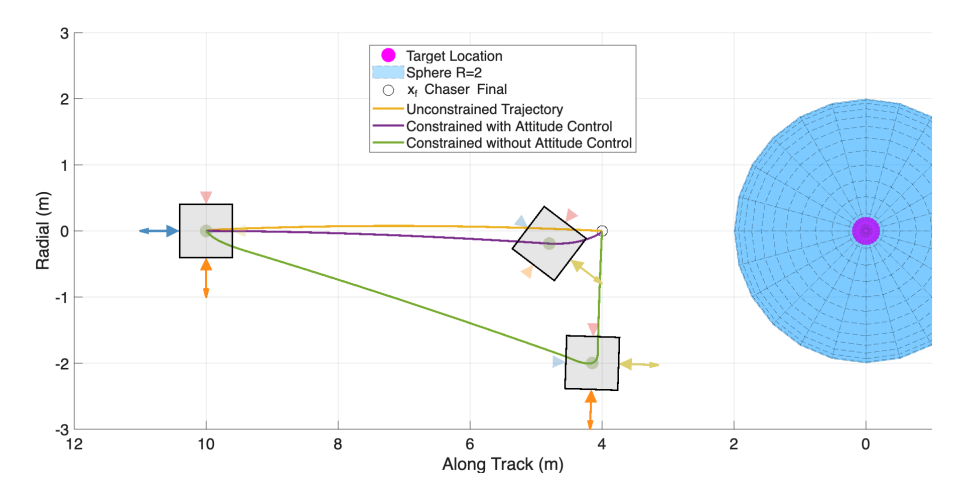
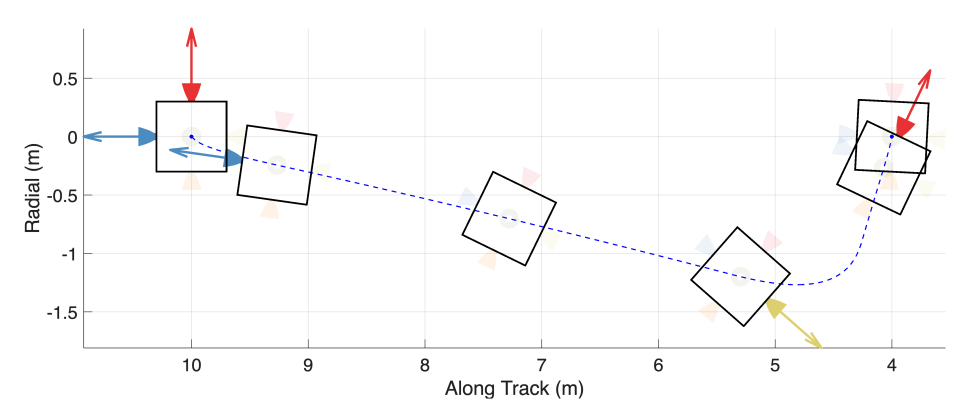


Figure 5: Comparison of results with snapshots of chaser orientation



**Figure 6**: Snapshots of chaser orientation (relative to target) during a constrained 6DOF problem with attitude control torque (R = 3.5m) at times t = 0, 7, 16, 25, 39, 48 sec.

Figure 6 shows the attitude manouevre performed by the chaser (rotating for the terminal burn) to reduce fuel consumption and satisfy the thruster pointing constraint. When the final MRP is fixed to zero, the chaser must arrive early at the terminal position with zero velocity to have enough time to rotate back to the required attitude. This necessitates a faster transfer and slightly higher fuel consumption when compared to the case with a free final attitude (see Figure 10). This slightly higher fuel consumption is still significantly lower than the case without attitude control torque (i.e. a 47% fuel saving). Note the slight rotation of the relative orientation of the chaser at the final position is due to the rotation of the LVLH frame during the transfer. Figure 7 shows a comparison of the yaw angle, angular velocity and torque over the transfer for different size constraint spheres. It is evident that as the sphere radius is increased, the chaser must rotate more to avoid firing at the target, requiring longer thrust arcs and more control torque.

To obtain the converged solutions presented in this paper it is necessary to perform multi-parameter continuation on  $\kappa$ ,  $\epsilon$  and  $\rho$  respectively. In our simulations, we start with a value of  $\kappa=1$  and sweep this down to  $\kappa=10^{-3}$ . Starting with a value of  $\kappa=1$  is similar to reducing the maximum torque available, and discourages the solver from performing arbitrary rotations and finding a local min-

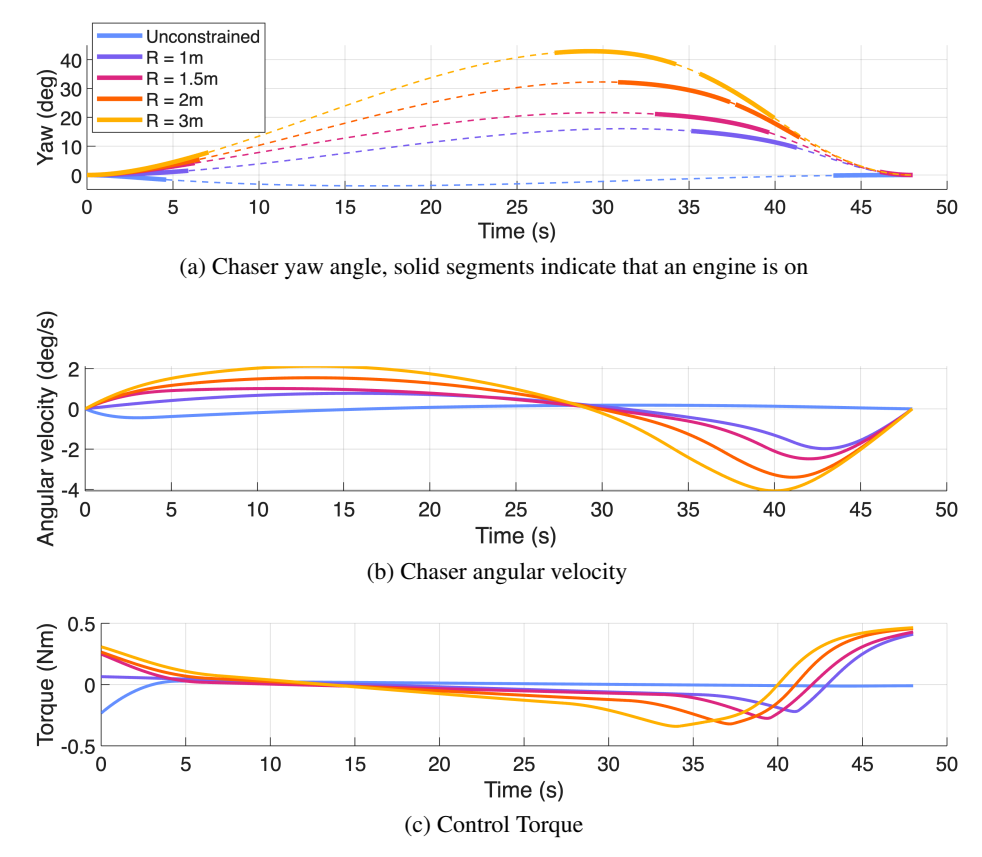


Figure 7: Chaser rotational motion with increasingly strict constraint region radius

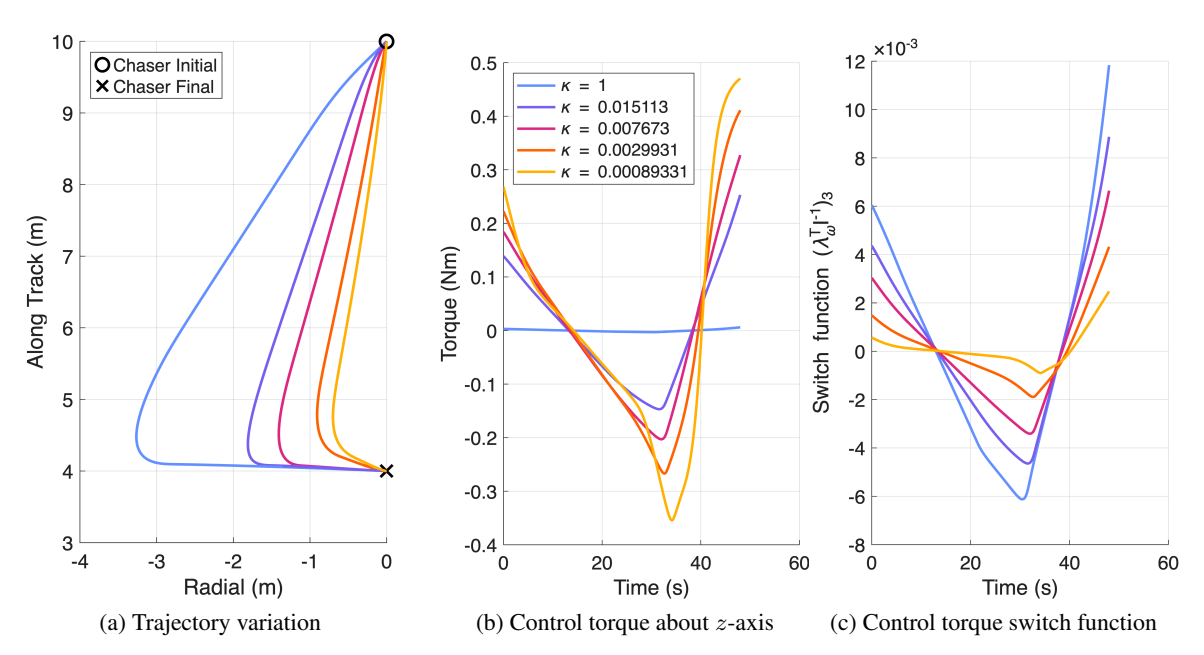
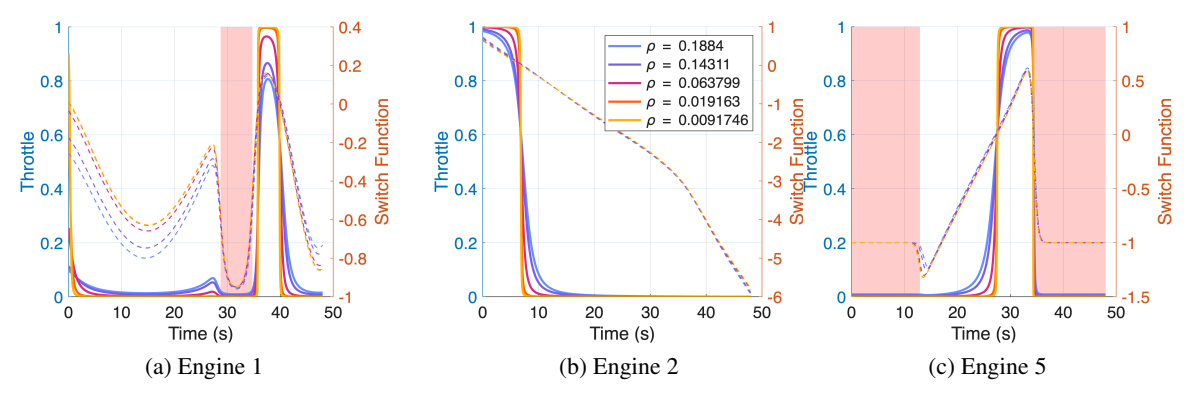


Figure 8: Effect of reducing  $\kappa$  on the trajectory, constraint Radius  $R=3.5 \mathrm{m}$ 

imum. At a value of  $\kappa=10^{-3}$ , the chaser has more control torque authority (singular torque is resolved), enabling a more efficient transfer. Note, if the chaser has fewer than 6 thrusters, the translational motion may not be controllable without torque, and we would need to start with a smaller value of  $\kappa$ , or start by solving problems where the control torque is penalized (as these are non-singular problems). The effect of the  $\kappa$  sweep on trajectory shape and control torque is shown in Figure 8a and 8b. Note the torque switch function for  $t \in [0,25]$  (Figure 8c) reduces in magnitude with  $\kappa$ , while the torque profile (on this segment) does not change, indicating a singular arc is present. We then make the pointing constraint more strict by sweeping  $\epsilon \to 10^{-2}$ , although this often has no effect as even a moderate reduction in thruster effectiveness causes the solver to avoid using a thruster. Finally, we reduce  $\rho \to 10^{-2}$  to approximate a bang-bang engine profile. Figure 9 shows the throttle profiles of the active engines (1,2,5), with shaded red regions indicating that a thruster would be violating the pointing constraint and is not permitted to fire. The converged values of the initial costates ( $\lambda_x(0)$ ) and homotopy parameters ( $\kappa$ ,  $\epsilon$ ,  $\rho$ ) for several cases presented in this section are given in Table 3.



**Figure 9**: Effect of reducing  $\rho$  on throttle profile, constraint Radius R=3.5m

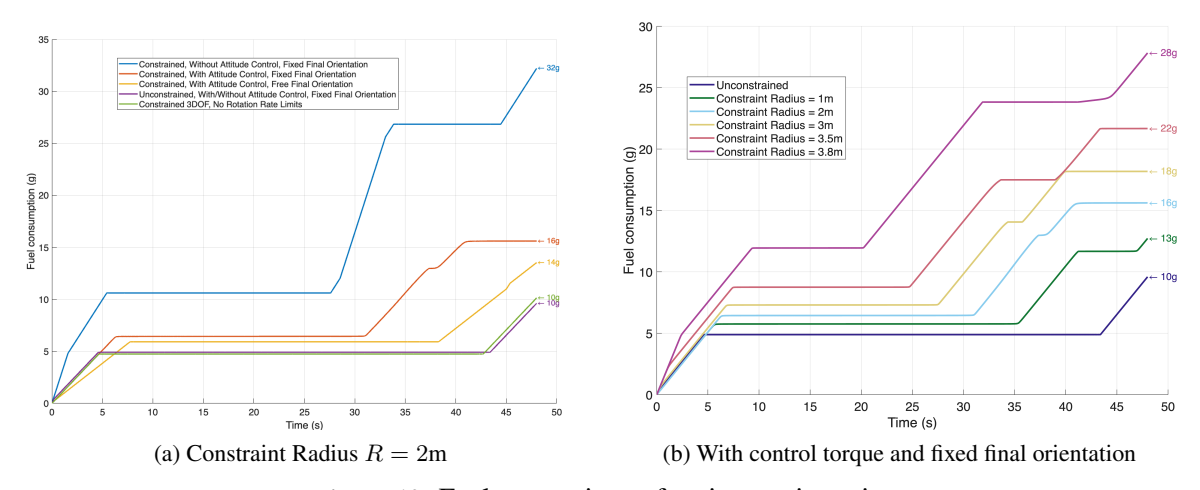


Figure 10: Fuel comparison of various trajectories

Figure 10a shows the variation in the propellant mass consumed for fuel-optimal trajectories with different constraints (i.e. active/inactive & fixed/free final boundary conditions) and available

control authority. These simulations consider spherical constraint of radius 2-meters. Figure 10b also shows propellant mass consumed, but for no-thrust spherical constraints of increasing radius. The time histories of the costates are presented in Figure 11. It is clear that the costates (including the MRP costates) for the fuel-optimal transfer are continuous, indicating that the MRPs did not contain any switches to the shadow set during our simulations. Additionally, the costates exhibit smooth behavior, as illustrated in the inset of Figure 11.

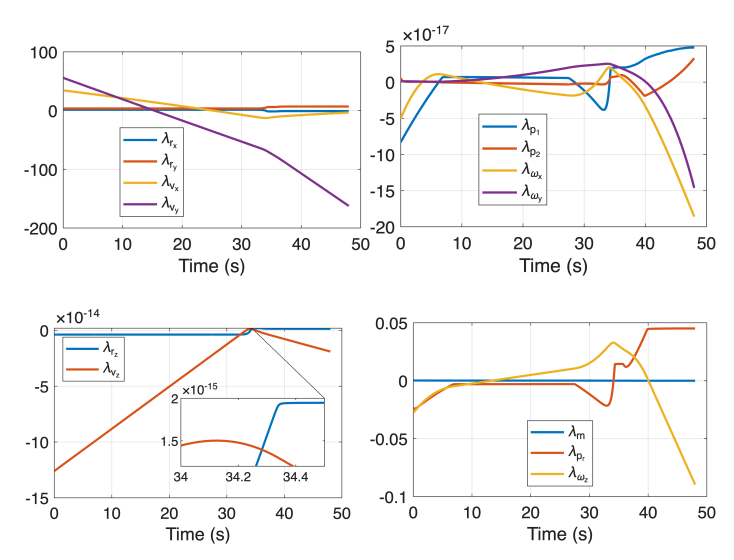


Figure 11: Costates for constrained approach with attitude control (R = 3m)

**Table 3**: Converged initial costates for the single shooting fuel-optimal problem with control torque

Variable	Unconstrained	R = 1m	R = 2m	R = 3m
$\overline{\rho}$	9.9092e-05	0.0096539	0.0096539	0.0091746
$\kappa$	0.00092413	0.00089331	0.00089331	0.00089331
$\epsilon$	0.5	0.0070715	0.0081743	0.0070715
$\lambda_{r_1}$	-0.706182604	-0.362565562	0.732702307	1.37948394
$\lambda_{r_2}$	1.77797982	2.4101687	3.08025246	3.5480307
$\lambda_{r_3}$	-5.51257611e-17	-1.25548985e-14	3.01654416e-16	1.36659668e-16
$\lambda_{v_1}$	-34.1516114	-5.05941283	30.7469978	34.2015753
$\lambda_{v_2}$	41.5788879	47.6102431	51.4354861	55.2911856
$\lambda_{v_3}$	-2.65056742e-15	-5.07779001e-13	1.08719111e-14	4.57478858e-15
$\lambda_m$	0.000106683928	0.000150830693	0.000191247664	0.000224251149
$\lambda_{p_1}$	-1.38230214e-18	-3.1322081e-16	7.21849712e-18	3.18403645e-18
$\lambda_{p_2}$	-6.85008808e-20	6.43625611e-19	-1.22846486e-19	-1.37454849e-19
$\lambda_{p_r}$	0.0167182194	0.00165502066	-0.0224886801	-0.0245702846
$\lambda_{\omega_x}$	-6.85776933e-19	-1.83586983e-16	4.54502214e-18	2.03103433e-18
$\lambda_{\omega_y}$	-4.71100059e-21	1.47832496e-20	-8.85212418e-20	1.14154433e-19
$\lambda_{\omega_z}$	0.00878291738	-0.00274171252	-0.0214464401	-0.0281054034

#### Validation of approach with 3DOF results

In this section we validate our approach against solutions of the simpler 3DOF problem detailed in. The specific transport of the 3DOF work, it is assumed the spacecraft is a point mass and that the thrust direction can change arbitrarily fast. As such, some differences are to be expected when compared to the 6DOF solutions. For this comparison study, we allowed the final orientation of the 6DOF problem be free in order for a fairer comparison to be made. Figure 12a and 12b show a quick (infeasibly) fast change in plume direction in the optimal 3DOF solution. This results in shorter burns arcs than for the 6DOF problem as indicated by solid lines in Figure 12b (3DOF) and Figure 12c (6DOF). Figure 12c shows that, by yawing about the z-axis, the chaser spacecraft uses two engines simultaneously during the terminal burn to achieve a similar acceleration to the one in Figure 12a. Finally, Figure 12d shows that only very small differences are apparent between the 3DOF and 6DOF trajectories.

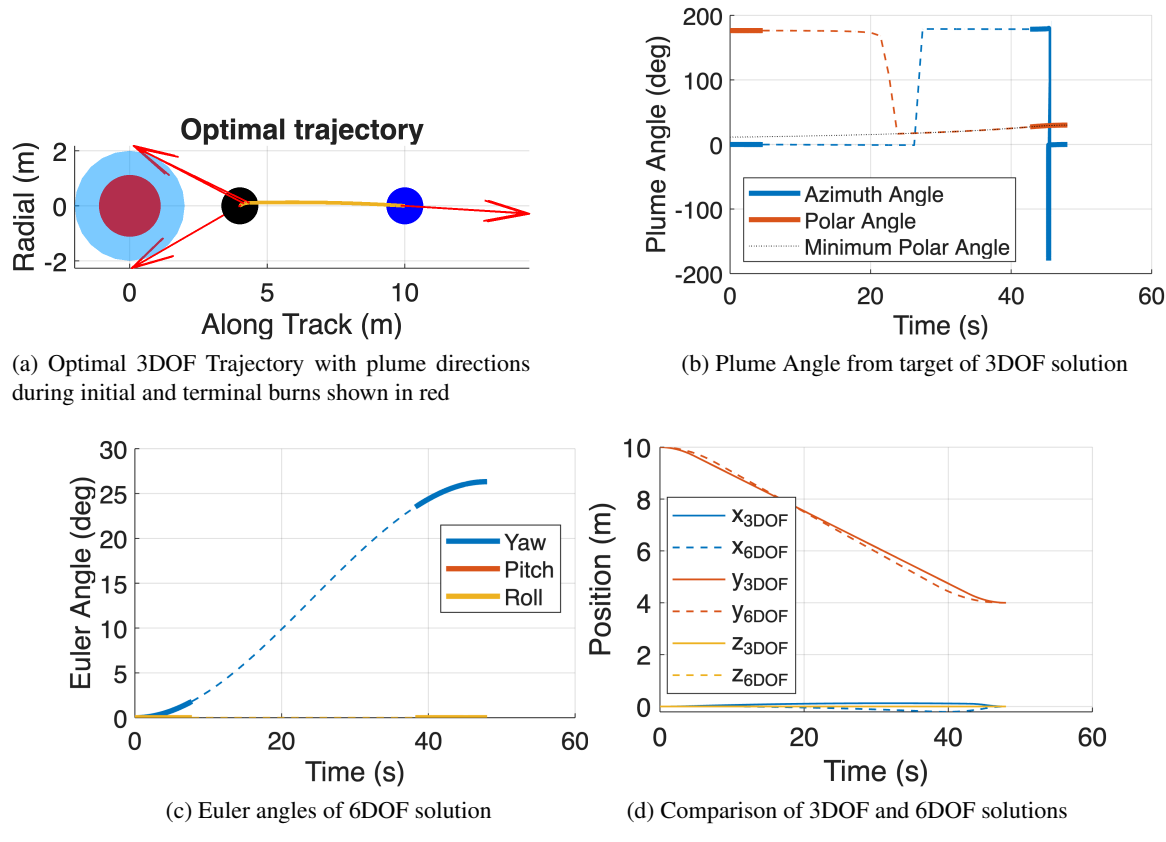


Figure 12: Solutions to the constrained 3DOF and 6DOF problem (R = 2m)

### **CONCLUSION**

We present a novel approach to incorporate a thruster pointing constraint into the 6DOF space-craft motion and solve the resulting trajectory optimization problem through use of the maximum principle. We focus on fuel optimality and do not penalize the control torque for the transfer, resulting in singular arcs which we address using L2Norm regularization.

Our approach avoids a multi-point boundary value problem and does not require a priori knowl-

edge the burn sequence or information regarding when the constraint is active or inactive. We demonstrated the practicality of the method by solving various fuel-optimal rendezvous trajectories under Clohessy-Wiltshire dynamics with different constraint strictness (target radius), spacecraft configuration (with and without reaction control torque), and boundary conditions (fixed/free final MRP). We validate our method against the simpler 3DOF problem and note that it is far simpler to incorporate torque limits and to compare thruster configurations. Our methodology can be applied to different dynamical regions, cost functions and chaser configurations, making it a useful tool for a variety of in-space assembly and servicing missions.

#### REFERENCES

- [1] L. S. Pontryagin, Mathematical Theory of Optimal Processes. CRC Press, 1987.
- [2] H. Panag, R. Woollands, S. Bandyopadhyay, and A. Rahmani, "Reducing Thruster Plume Contamination for Satellite Servicing Using Convex Optimization," *American Astronautical Society Guidance, Navigation and Controls Conference*, 2023.
- [3] Y. Zhang, B. Zhu, M. Cheng, and S. Li, "Trajectory optimization for spacecraft autonomous rendezvous and docking with compound state-triggered constraints," *Aerospace Science and Technology*, Vol. 127, 2022, p. 107733, 10.1016/j.ast.2022.107733.
- [4] X. Liu and P. Lu, "Solving nonconvex optimal control problems by convex optimization," *Journal of Guidance, Control, and Dynamics*, Vol. 37, No. 3, 2014, pp. 750–765, 10.2514/1.62110.
- [5] S. Mitani and H. Yamakawa, "Continuous-thrust transfer with control magnitude and direction constraints using smoothing techniques," *Journal of Guidance, Control, and Dynamics*, Vol. 36, No. 1, 2013, pp. 163–174, 10.2514/1.56882.
- [6] A. E. Bryson and Y. C. Ho, Applied Optimal Control. New York: Blaisdell, 1969.
- [7] H. Panag and R. Woollands, "Thruster-Pointing-Constrained Optimal Control for Satellite Servicing Using Indirect Optimization," *Journal of Spacecraft and Rockets*, Vol. 0, No. 0, 0, pp. 1–13, 10.2514/1.A36064.
- [8] M. D. Shuster *et al.*, "A survey of attitude representations," *Navigation*, Vol. 8, No. 9, 1993, pp. 439–517.
- [9] S. Marandi and V. Modi, "A preferred coordinate system and the associated orientation representation in attitude dynamics," *Acta Astronautica*, Vol. 15, Nov. 1987, pp. 833–843, 10.1016/0094-5765(87)90038-5
- [10] H. Schaub, J. L. Junkins, and R. D. Robinett, "New Penalty Functions and Optimal Control Formulation for Spacecraft Attitude Control Problems," *Journal of Guidance, Control, and Dynamics*, Vol. 20, May 1997, pp. 428–434, 10.2514/2.4093.
- [11] K. D. Bilimoria and B. Wie, "Time-optimal three-axis reorientation of a rigid spacecraft," *Journal of Guidance, Control, and Dynamics*, Vol. 16, No. 3, 1993, pp. 446–452, 10.2514/3.21030.
- [12] H. Shen and P. Tsiotras, "Time-Optimal Control of Axisymmetric Rigid Spacecraft Using Two Controls," *Journal of Guidance, Control, and Dynamics*, Vol. 22, Sept. 1999, pp. 682–694, 10.2514/2.4436.
- [13] R. Bommena and R. Woollands, "Indirect Trajectory Optimization with Path Constraints for Multi-Agent Proximity Operations," *The Journal of the Astronautical Sciences*, Vol. 71, No. 6, 2024, p. 54, 10.1007/s40295-024-00470-7.
- [14] C. Silva and E. Trelat, "Smooth regularization of bang-bang optimal control problems," *IEEE Transactions on Automatic Control*, Vol. 55, No. 11, 2010, pp. 2488–2499, 10.1109/TAC.2010.2047742.
- [15] K. Mall and M. J. Grant, "Epsilon-Trig Regularization Method for Bang-Bang Optimal Control Problems," *Journal of Optimization Theory and Applications*, Vol. 174, No. 2, 2017, pp. 500–517, 10.1007/s10957-017-1129-9.
- [16] I. Introdcctiok, "Computation of Optimal Singular Controls," *Trial*, No. February, 1970, pp. 67–73.
- [17] K. Mall and E. Taheri, "Unified trigonometrization method for solving optimal control problems in atmospheric flight mechanics," AIAA Scitech 2020 Forum, No. January, 2020, pp. 1–18, 10.2514/6.2020-0022.
- [18] E. Taheri and N. Li, "L2 Norm-Based Control Regularization for Solving Optimal Control Problems," *IEEE Access*, Vol. 11, No. November, 2023, pp. 125959–125971, 10.1109/access.2023.3331382.
- [19] W. H. Clohessy and R. S. Wiltshire, "Terminal Guidance System for Satellite Rendezvous," *Journal of the Aerospace Sciences*, Vol. 27, No. 9, 1960, pp. 653–658, 10.2514/8.8704.

- [20] F. L. Markley and J. L. Crassidis, Fundamentals of Spacecraft Attitude Determination and Control. Space Technology Library, Springer New York, NY, 1 ed., 2014, 10.1007/978-1-4939-0802-8.
- [21] H. D. Curtis, *Orbital Mechanics for Engineering Students*. Elsevier Butterworth Heinemann, 2020, 10.1016/c2016-0-02107-1.
- [22] J. E. Prussing, "Primer vector theory and applications," *Spacecraft trajectory optimization*, Vol. 29, 2010, p. 16.
- [23] R. Bertrand and R. Epenoy, "New smoothing techniques for solving bang-bang optimal control problems Numerical results and statistical interpretation," *Optimal Control Applications and Methods*, Vol. 23, No. 4, 2002, pp. 171–197, 10.1002/oca.709.
- [24] E. Taheri and J. L. Junkins, "Generic Smoothing for Optimal Bang-Off-Bang Spacecraft Maneuvers," *Journal of Guidance, Control, and Dynamics*, Vol. 41, No. 11, 2018, pp. 2470–2475, 10.2514/1.G003604.
- [25] E. R. Pager and A. V. Rao, "Minimum-Time Reorientation of Axisymmetric Rigid Spacecraft Using Three Controls," *Journal of Spacecraft and Rockets*, Vol. 59, Nov. 2022, pp. 2195–2201, 10.2514/1.A35422.